

https://doi.org/10.1070/QEL17960

Study of adsorption of the SARS-CoV-2 virus spike protein by vibrational spectroscopy using terahertz metamaterials

M.R. Konnikova, O.P. Cherkasova, T.A. Geints, E.S. Dizer, A.A. Man'kova, I.S. Vasilievskii, A.A. Butylin, Yu.V. Kistenev, V.V. Tuchin, A.P. Shkurinov

Abstract. **Adhesion of the spike protein of the SARS-CoV-2 virus is studied by vibrational spectroscopy using terahertz metamaterials. The features of metastructure absorption upon the deposition of histidine, albumin, and the receptor-binding domain of the spike protein films are investigated. An original technique for quantitative assessment of the efficiency of virus adhesion on the metamaterial surfaces are proposed and experimentally tested.**

Keywords: *metamaterials, terahertz spectroscopy, viruses, adhesion.*

1. Introduction

In March 2020, the World Health Organization recognised the infectious disease COVID-19 caused by the SARS-CoV-2 coronavirus as a pandemic. The outer envelope of the virus is formed by a spike (S) protein, the main functions of which are specific binding to membrane receptors of cells and adhesion to various physical surfaces [1–4]. The spike protein consists of two subunits, S1 and S2. The S1 subunit, including the receptor binding domain (RBD), is responsible for binding to surfaces [5]. It is assumed that the interaction of the virus with the surface is largely due to weak nonspecific intermolecular interactions, including hydrogen bonds [6]. The relaxation times of hydrogen bonds correspond to the terahertz (THz) range. The current level of development of the technology for generating and detecting THz radiation, as well as the methods of its application in biophotonics [7], suggests the possibility of using the THz photonics to study the peculiarities of adhesion of the spike protein of the SARS-CoV-2 virus.

An earlier study of the contagiousness of the SARS-CoV-2 virus showed [8] that the survival rate (titre threshold) of the virus depends on the physicochemical properties of the surface. Moreover, the survival rate on metal surfaces is also different for different types of metals. In this regard, there is a need to understand the physical mechanisms that ensure the interaction of the RBD S protein with metal surfaces that have different physicochemical properties.

The methods of low-frequency vibrational spectroscopy play an important role in studying the mechanisms of interaction of complex molecular systems with a surface. IR spectroscopy and Raman spectroscopy (RS) are sensitive to intramolecular vibrations and rotations of isolated molecular groups of a large number of complex molecules, as well as to conformational changes in protein molecules during interactions with other molecules, in particular during early detection of various diseases [9–12]. The use of Raman and IR Fourier transform spectroscopy is well known for studying the structure and functions of proteins [9–11], as well as for detecting and identifying viruses [12]. THz time-domain spectroscopy (THz-TDS) belongs to the modern methods of vibrational spectroscopy in the region of low interaction energies, which makes it possible to analyse intermolecular vibrational motions, including those associated with the breaking and formation of low-energy hydrogen bonds [7, 13, 14]. The mechanism of the formation of hydrogen bonds during the interaction of proteins with the surface, observed in the THz range, will serve as a selective marker in the study of protein adhesion.

To increase the sensitivity of spectroscopic methods to the study of thin molecular layers, waveguide and plasmon devices are widely used [15–18]. To date, such plasmonics-based spectroscopic methods are known as surface-enhanced Raman spectroscopy (SERS) [19], surface-enhanced IR absorption spectroscopy (SEIRA) [20], and enhanced THz

M.R. Konnikova, T.A. Geints Faculty of Physics, Lomonosov Moscow State University, Leninskie Gory, 119991 Moscow, Russia; Institute on Laser and Information Technologies, Branch of the Federal Research Centre 'Crystallography and Photonics', Russian Academy of Sciences, Svyatoozerskaya ul. 1, 140700 Shatura, Moscow region, Russia; e-mail: konnikovamaria@gmail.com;
O.P. Cherkasova Institute on Laser and Information Technologies, Branch of the Federal Research Centre 'Crystallography and Photonics', Russian Academy of Sciences, Svyatoozerskaya ul. 1, 140700 Shatura, Moscow region, Russia; Institute of Laser Physics, Siberian Branch, Russian Academy of Sciences, prosp. Akad. Lavrentieva 15B, 630090 Novosibirsk, Russia; National Research Tomsk State University, prosp. Lenina 36, 634050 Tomsk, Russia;
E.S. Dizer Institute on Laser and Information Technologies, Branch of the Federal Research Centre 'Crystallography and Photonics', Russian Academy of Sciences, Svyatoozerskaya ul. 1, 140700 Shatura, Moscow region, Russia; National Research Nuclear University MEPhI, Kashirskoe sh. 31, 115409 Moscow, Russia;
A.A. Man'kova, A.A. Butylin Faculty of Physics, Lomonosov Moscow State University, Leninskie Gory, 119991 Moscow, Russia;
I.S. Vasilievskii National Research Nuclear University MEPhI, Kashirskoe sh. 31, 115409 Moscow, Russia;
Yu.V. Kistenev National Research Tomsk State University, prosp. Lenina 36, 634050 Tomsk, Russia;
V.V. Tuchin National Research Tomsk State University, prosp. Lenina 36, 634050 Tomsk, Russia; Saratov State University, ul. Astrakhanskaya 83, 410012 Saratov, Russia; Institute for Problems of Precision Mechanics and Control, Russian Academy of Sciences, ul. Rabochaya 24, 410028 Saratov, Russia;
A.P. Shkurinov Faculty of Physics, Lomonosov Moscow State University, Leninskie Gory, 119991 Moscow, Russia; Institute on Laser and Information Technologies, Branch of the Federal Research Centre 'Crystallography and Photonics', Russian Academy of Sciences, Svyatoozerskaya ul. 1, 140700 Shatura, Moscow region, Russia; National Research Tomsk State University, prosp. Lenina 36, 634050 Tomsk, Russia

Received 20 September 2021
Kvantovaya Elektronika **52** (1) 2–12 (2022)
Translated by V.L. Derbov

spectroscopy using artificial metamaterials [15–17, 21–24]. In this work, we propose a new metamaterial, which is a combination of the previously described two-dimensional metal structures on a dielectric substrate [25]. We assume that this metamaterial will make it possible to study the adhesion properties of viruses to a metal surface in the THz range.

Thus, the main goal of our work is to study the adhesion properties of RBD S protein by vibrational spectroscopy, namely, THz spectroscopy. The features of vibrational spectroscopy of thin molecular layers determine the use of methods for amplifying the local field to increase the sensitivity and selectivity of spectroscopic techniques. The paper demonstrates the efficiency of using two-dimensional metamaterials to study the adhesive properties of viral proteins. A practical method of using metamaterials is also proposed. For comparison, we studied the adhesive properties of bovine serum albumin (BSA), which is close in molecular weight and structure to the S-protein, and the amino acid histidine, the use of which made it possible to demonstrate the effectiveness of the proposed method for studying the specific features of the interaction of complex molecules with surfaces.

2. Materials and methods

In this work, we used commercial preparations of BSA and histidine (Sigma, USA). RBD of the SARS-CoV-2 virus was obtained from the Chinese hamster ovary (CHO) recombinant line, purified and offered by D.V. Shcheblyakov, a researcher of the Gamaleya Research Institute of Epidemiology and Microbiology.

First, films were deposited on pure silicon or on a metastructure, then the film thickness was measured, and finally absorption was measured with a THz time-domain spectrometer [26, 27]. Sample preparation stages are shown in Fig. 1. Their detailed description will be given below.

2.1. Sample preparation by the 'immersion in solution' method

The obtained samples of silicon or metastructure were immersed in an aqueous solution of the substances studied. The concentration of the solutions was 0.14 mg mL^{-1} for histidine, 0.645 mg mL^{-1} for BSA, and 3.5 mg mL^{-1} for RBD. The time of keeping the samples in the solution was 5 s, then the sample was taken out and dried for 5 min at a temperature of 22 °C. After each drying, the absorption of THz radiation by the sample was measured. Samples were immersed in each solution five times.

2.2. Sample preparation by the sublimation method

The sublimation method is based on a first-order phase transition from the crystalline state of a substance to the gas phase, followed by deposition on the structure under study

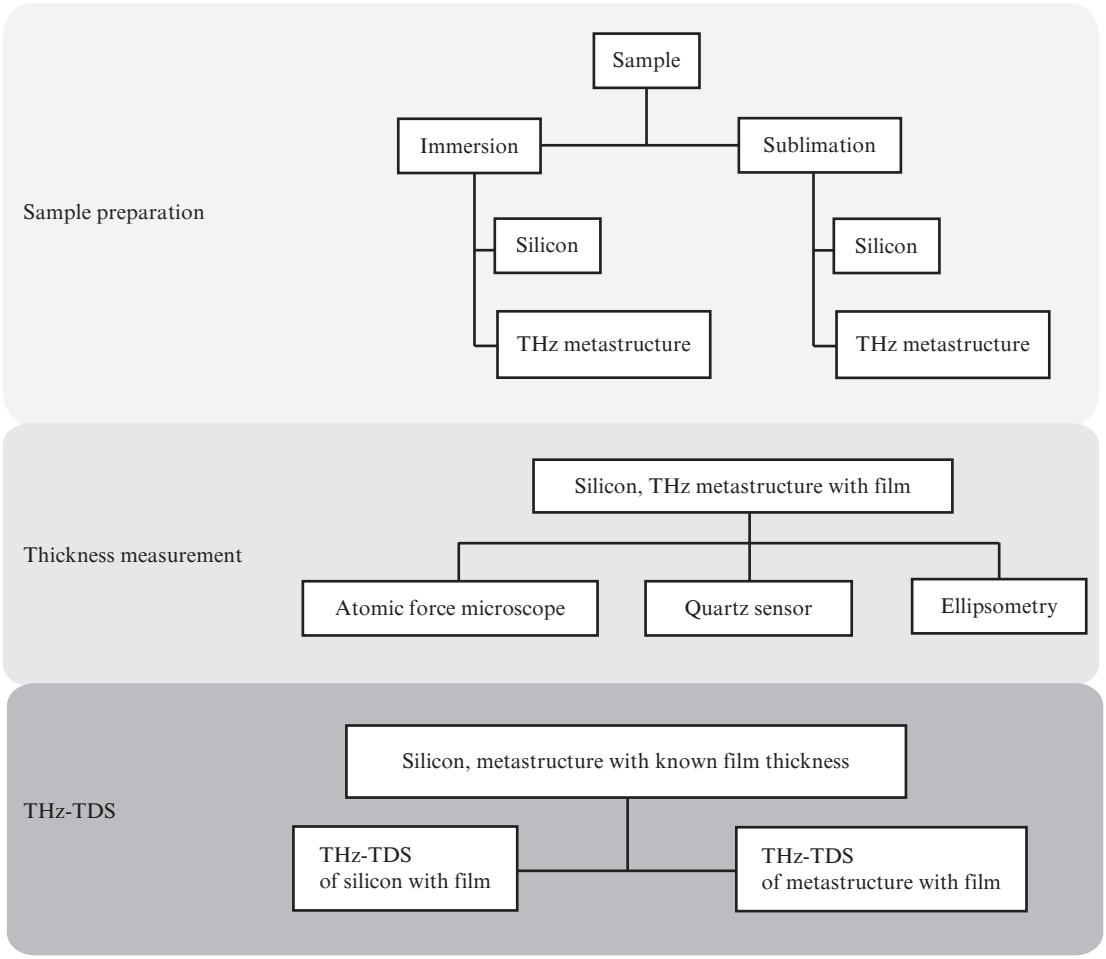

Figure 1. Sample preparation technique for THz-TDS.

[28]. This method was used to deposit histidine films under vacuum conditions. The process was carried out using a cell for the sublimation of organic materials (OME 40-2-25-S, Dr. Eberl MBE-Komponenten GmbH, Germany). Histidine was placed in a cell in an ultrahigh vacuum – 6×10^{-8} mbar. Samples placed in the same vacuum chamber were subjected to preliminary annealing at a temperature of 150 °C. The cell with histidine was heated up to a sublimation temperature of 186 °C. The thickness of the histidine layer, measured with a quartz sensor, linearly depends on the sublimation time, as shown in Fig. 2. The figure also shows an image of the metastructure obtained using an optical microscope with a magnification of 100×, with histidine deposited on it during 40 and 75 min.

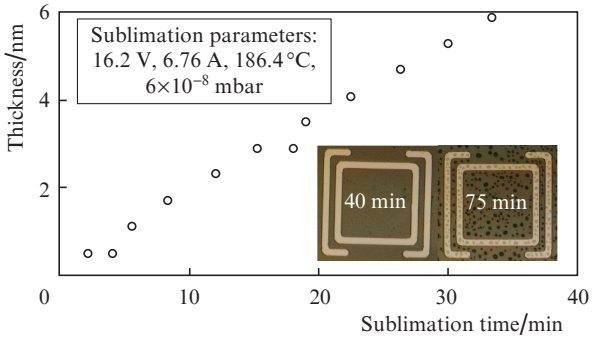

Figure 2. Film thickness versus sublimation time. The inset shows an image of a metastructure with a histidine film deposited on it, obtained using an optical microscope with a magnification of 100×, the film deposition time being 40 and 75 min.

2.3. Film thickness determination method

The thickness of the films was determined by three independent methods: using a vacuum atomic force microscope (VT-AFM XA, Omicron), a quartz sensor (STM-100/MF, Sycon) for deposited films, and ellipsometry method (SE400adv, Sentech). Note that when the metastructure and silicon were immersed in solutions of histidine, BSA, and RBD S protein, the thickness was measured only by the ellipsometry method.

Ellipsometry allows analysing the complex reflectance based on the tangent of the angle $\tan\Psi(\lambda)$, equal to the ratio of the attenuation of the scalar amplitudes of the s and p components, as well as the phase shift $\Delta(\lambda)$. These quantities cannot be directly converted into optical parameters, and, therefore, an approximation of the experimental data is required. As the latter, we used the Cauchy model [29]:

$$n(\lambda) = A + \frac{B}{\lambda^2} + \frac{C}{\lambda^4}, \tag{1}$$

$$k(\lambda) = 0, \tag{2}$$

where A, B and C are fitting parameters; and $n(\lambda)$ and $k(\lambda)$ are the real and imaginary parts of the refractive index. In this case, the film thickness d is determined from the relation:

$$\tan\Psi(\lambda)\exp[i\Delta(\lambda)] = F(N_s(\lambda), N_f(\lambda), \frac{d}{\lambda}), \tag{3}$$

where $N_s(\lambda) = n_s(\lambda) - ik_s(\lambda)$ and $N_f(\lambda) = n_f(\lambda) - ik_f(\lambda)$ are the complex refractive indices of the substrate and film, respectively.

2.4. IR spectroscopy method

The IR transmission spectrum of RBD S protein in the form of a lyophilised powder was measured using a commercial Nicolet 6700 spectrometer with a spectral range of 50–4000 cm^{-1} in transmission mode.

2.5. THz-TDS methods

Intermolecular interactions were studied using a THz time-domain spectrometer fabricated at the Lomonosov Moscow State University, the design and characteristics of which were described in detail in [26, 27]. Sample characteristics were measured in transmission mode.

At a THz pulse energy of 10^{-1} pJ, the experimental signal-to-noise ratio was 10^2 in the 0.2–2.5 THz range with a spectral resolution of 20 GHz. The humidity inside the THz spectrometer was 30 %. The spectral characteristics of the samples in the indicated range were calculated based on the formulae below.

The dependence of the field amplitude on the frequency $E(f)$ is determined using the Fourier transform of the time profile of the THz pulse $E(t)$:

$$E(f) = \mathrm{FFT}(E(t)). \tag{4}$$

The transmittance of the sample is calculated as the ratio of the field amplitude passing through the sample to the field amplitude in the absence of the sample (reference signal):

$$T(f) = \frac{E_{sam}(f)}{E_{ref}(f)}. \tag{5}$$

Hence, for the absorption index of the sample α, we obtain the expression

$$\alpha = \frac{-\ln[T(f)] + \ln(1 - R^2)}{d}, \tag{6}$$

where $R = (n_{av} - 1)/(n_{av} + 1)$ is the reflection coefficient; $n_{av} = 1 + \Delta tc/d$ is the average refractive index; and Δt is the delay of the pulse when passing through the sample.

2.6. Preparation of THz metamaterials

To increase the sensitivity of THz spectroscopy to the presence of RBD S protein molecules on the surface, a metastructure was developed, which has two absorption resonances at frequencies of 0.85 and 1.06 THz. The calculation of the metastructure parameters, as well as its main optical and electromagnetic characteristics was carried out in the CST Studio Suite software package. The metastructure is a two-dimensional structure consisting of a silicon substrate 300 μm thick and an aluminium layer 200 nm thick in the form of a pattern (an array of figures). Since silicon is transparent in the THz range, it is used as a substrate [30]. The pattern should be made of a material with high conductivity and complex dielectric constant in the THz frequency range. Metals such as gold and aluminium meet these requirements [22, 24].

Despite the fact that the conductivity and complex dielectric constant of gold are higher, in this work the pattern is made of aluminium, because this material is more economical, and the presence of oxide on its surface can be taken into account at the stage of structure modelling [31]. We chose a modified pattern of split-ring resonators (SRRs), consisting of a square inner ring and an outer half-ring, since the reasons for the appearance of resonances for this pattern are well studied [32, 33]. In addition, this type of metastructure allows the creation of resonances in absorption spectra that are sensitive to the presence of films. This is possible due to the high concentration of the electric field lines in the gap regions, which gives rise to narrow resonances in the THz absorption spectra. The geometry of the structure is shown in Fig. 3. The structures were fabricated by explosive metallisation (liftoff) with a LOR9/S1813 double-layer photoresist mask exposed using contact photolithography (Suss MJB4) at the National Research Nuclear University MEPhI. The deposition of aluminium was carried out by the method of vacuum thermal sputtering on a Kurt Lesker PVD75 facility at a residual gas pressure of 10^{-6} Torr.

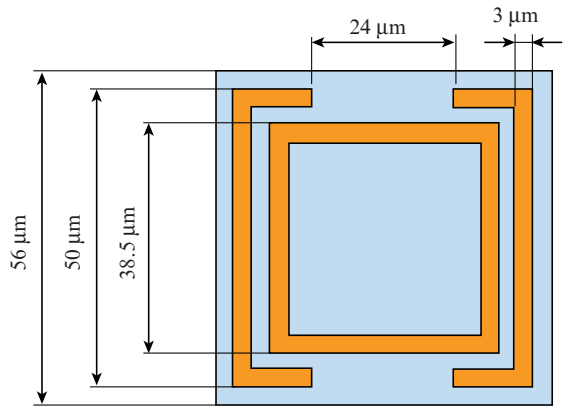

Figure 3. Geometry of the THz metastructure. The substrate material is silicon; the material of the conductive layer is aluminium.

3. Results and discussion

3.1. IR spectroscopy of RBD S protein

The nature of intramolecular interactions is associated with molecular vibrations. The presence of characteristic lines in the IR spectra indicates the presence of the corresponding atomic group or bond in the molecule. In the case of proteins, the study of vibration processes in a molecule makes it possible to obtain information about its conformational modifications [8].

It was mentioned earlier that the method of IR spectroscopy makes it possible to study the intramolecular interactions inherent in a particular molecule. The spectra of both the S, S1 proteins and the RBD S protein of the SARS-CoV-2 virus were studied by IR spectroscopy earlier [34]. However, the results of IR spectroscopy for the RBD S protein obtained from the CHO culture are currently absent in the literature; therefore, the IR absorption spectrum of this substance is presented for the first time in this work in Fig. 4. The positions of most of the absorption lines (at frequencies of 949, 1159, 1467, and 1699 cm^{-1}) coincide with those given in Ref. [34], where the RBD S protein obtained from other cultures was studied. The main differences appear in the range 3250–3500 cm^{-1}, which corresponds to the stretching of the O–H bond.

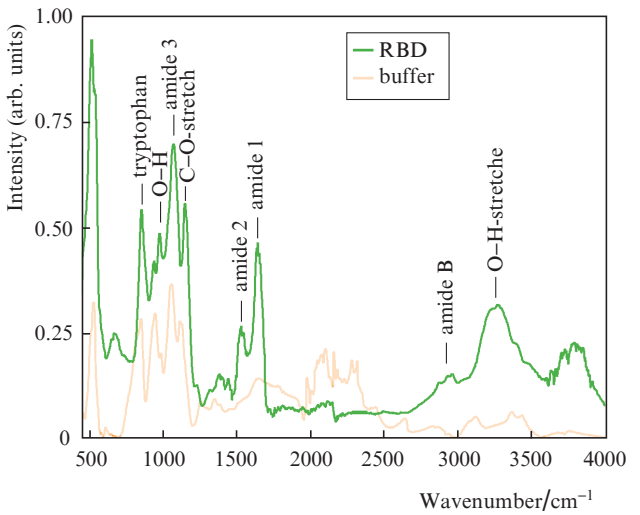

Figure 4. (Colour online) Absorption spectrum of the RBD S protein with indication of functional groups.

3.2. THz-TDS of RBD solutions and films

Since low-energy hydrogen interactions occur in the THz range, THz spectroscopy can be used as a method for detecting intermolecular interactions. We have previously shown that THz spectroscopy is sensitive to relaxation processes occurring in protein solutions [35–37]. A noticeable and reproducible effect of protein on the THz response of water is observed at protein concentrations above 10 mg mL^{-1} [36]. The absorption indices of water, solutions of histidine, BSA, and RBD, averaged over three measurements, were calculated using Eqns (4)–(6) and are shown in Fig. 5. It can be seen that the differences in the absorption indices of water and solutions are less than the measurement error. This suggests that, without additional methods of field amplification, THz-TDS cannot give a reliable result when analysing vibrational spectra in solutions with a low concentration of the substances under study.

We also measured the THz absorption of a 380-μm-thick pure silicon substrate. Then it was immersed in previously measured solutions of histidine, BSA and RBD. Figure 6 shows the absorption spectra of thin films of histidine, BSA, and RBD deposited on a silicon substrate. The differences in these spectra are small, which makes it impossible to identify differences in the transmission spectra of films of different thicknesses. In this regard, the study of thin films by the method of THz-TDS is not possible, since the contribution of thin films to the total spectrum is too small.

3.3. THz spectroscopy of RBD S protein films deposited on metamaterials

To increase the sensitivity of vibrational spectroscopy methods, new methods based on plasmonics have been developed, for example, SERS [19], SEIRA [20], and THz sensorics [21–24], which make it possible to increase the response signal from the substance applied to the sensor, by tens to thou-

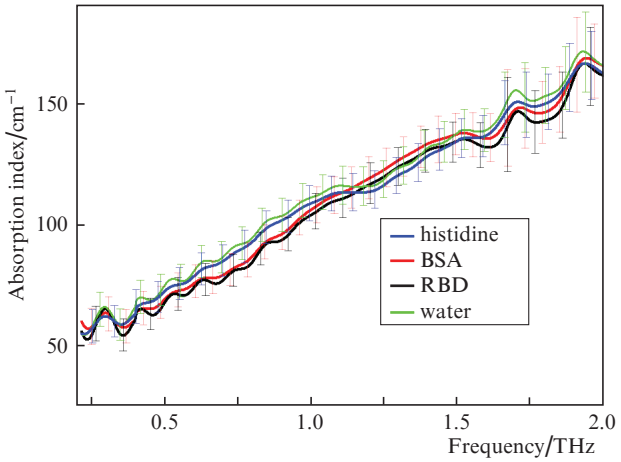

Figure 5. (Colour online) Absorption index spectra of water, solutions of histidine, BSA and RBD with the error of averaging over three measurements. The thickness of the solution layer is 0.21 mm.

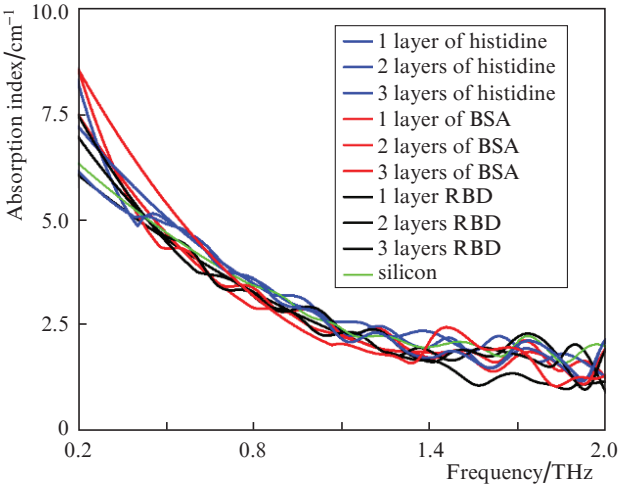

Figure 6. (Colour online) Absorption index spectra of histidine, BSA, and RBD films of different thicknesses deposited on high-resistance silicon.

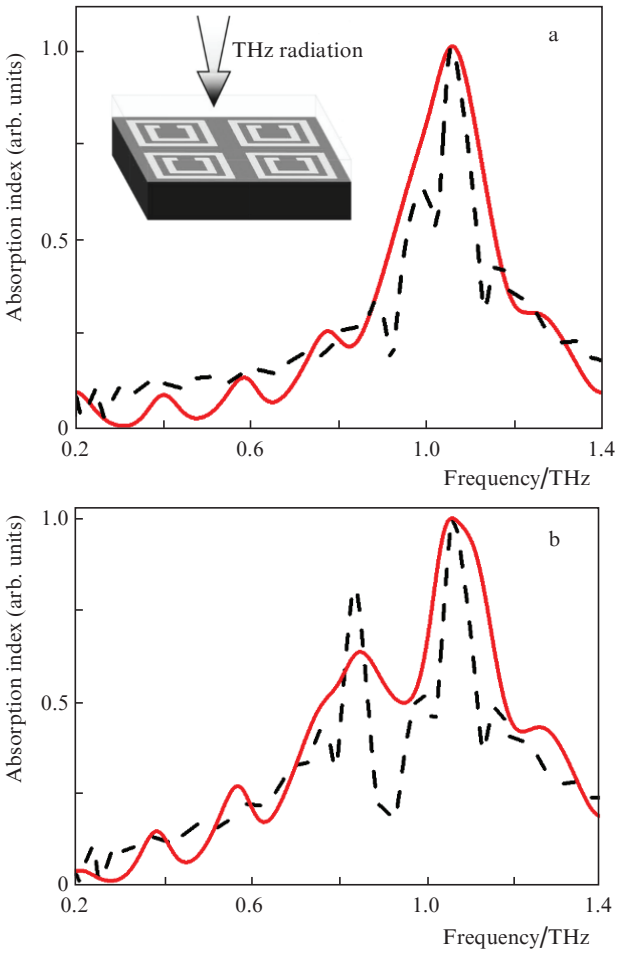

Figure 7. (Colour online) Normalised absorption index spectra of the THz metastructure for (a) p-polarised and (b) s-polarised THz waves, obtained in theoretical modelling (solid curves) and experiment (dashed curves).

sands times. We study the adhesion properties of the RBD viral S-protein, BSA and histidine using THz-TDS in combination with metastructures adapted for the THz frequency range. The adhesion mechanism is based on the formation of hydrogen bonds between RBD and the metal surface of the metastructure.

Figure 7 shows the results of computer simulation of the absorption index of the metastructure and its experimental spectrum in the range 0.2–1.4 THz. The experimental data repeat the simulation data with high accuracy. By high accuracy, we mean the degree of coincidence of resonances, which is calculated as $F_{mod}/F_{exp} \times 100\%$ and amounted to 99.6% ± 0.1%.

The structure we have developed has two resonances in the absorption spectra. The resonance at a frequency of 0.85 THz is excited in the region of the gap and is called inductor- capacitor resonance (*LC* resonance), which arises from the accumulation of charge in this region on the outer ring. The dipole resonance at a frequency of 1.06 THz is due to the lattice constant of two conducting circuits and does not depend on the polarisation of the incident THz wave [38].

Based on the dielectric characteristics of the metastructure materials (conductivity, permittivity), its dimensions, as well as taking into account the direction of propagation of radiation and its polarisation, the electric field distribution on the developed metastructure surface at frequencies of 0.85 and 1.06 THz was simulated (Fig. 8). From the data on the electric field distribution on the metastructure surface, it can be seen that the maximum at a frequency of 0.85 THz is polarisation-dependent. This is due to the asymmetry of the structure, which creates a resonance at the indicated frequency. The calculated electric field strength at a frequency of 1.06 THz is ~128 V m^{-1} for both s- and p-polarised incident radiation.

The developed metastructure, in comparison with the one presented in Ref. [39], demonstrates a higher field strength in the region of the gap at resonance frequencies. Moreover, such a metastructure has two resonance frequencies, the mechanisms of the changes in which are different for each type of film, in contrast to metastructures with one resonance frequency [16].

Figure 9 shows the results of an experiment on measuring the absorption index of a metastructure with deposited histidine, BSA, and RBD films of various thicknesses. A shift of the resonance frequency to the low frequency region and an

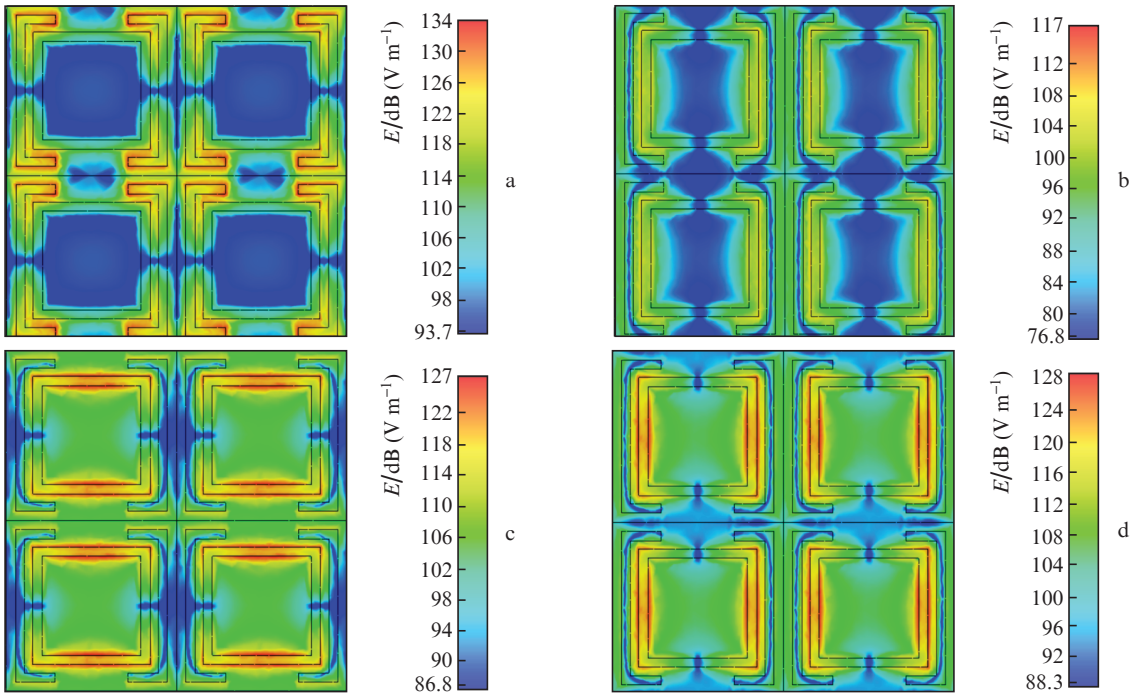

Figure 8. (Colour online) Electric field strength E at the metastructure resonance frequencies of (a, b) 0.85 and (c, d) 1.06 THz with (a, c) s-polarisation and (b, d) p-polarisation.

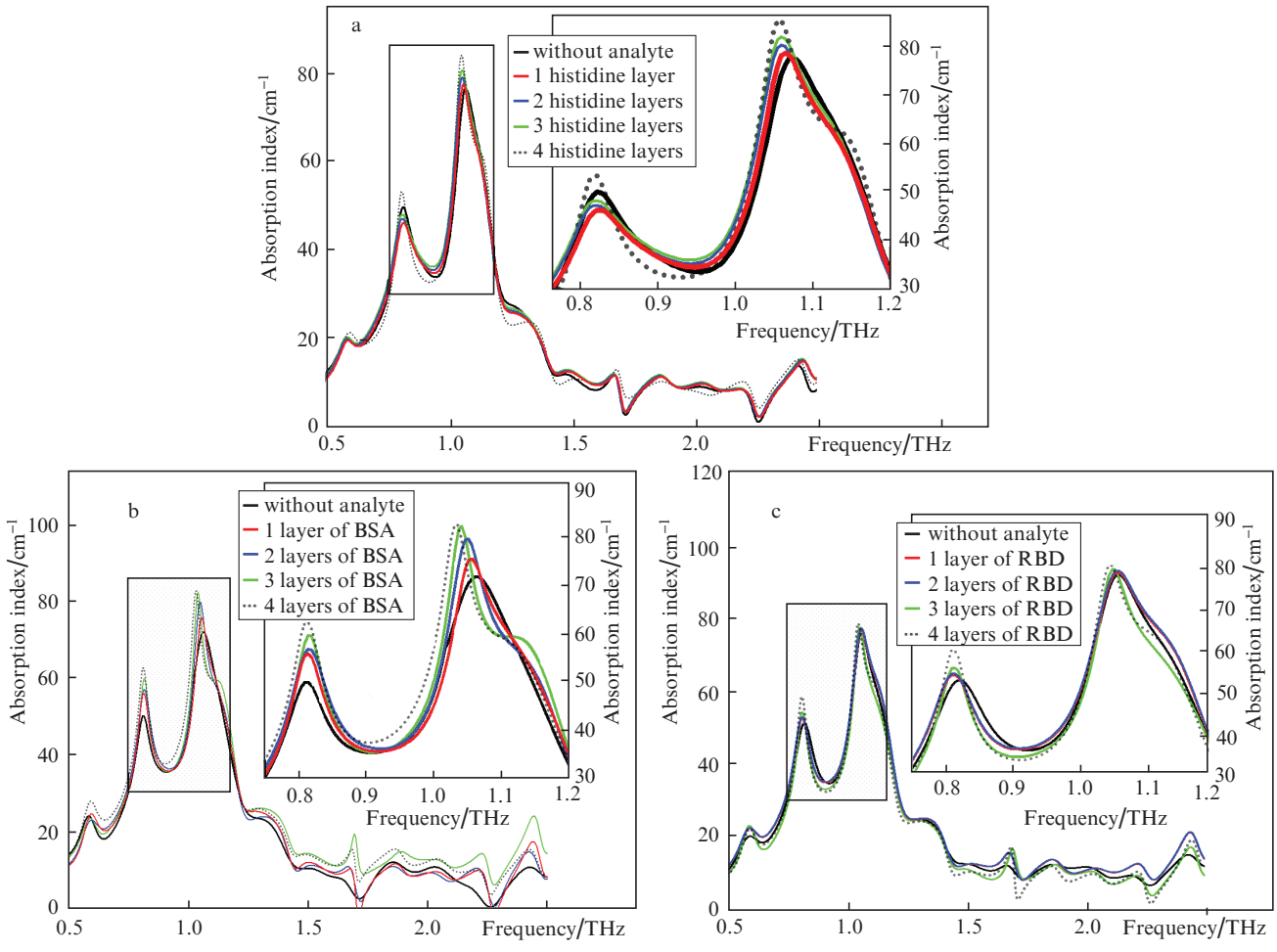

Figure 9. (Colour online) Absorption index spectra of the metastructure with deposited films of (a) histidine, (b) BSA, and (c) RBD S protein.

increase in the absorption index are observed for each resonance, due to an increase in the layer thickness of different substances with their characteristic permittivities. In addition, as the film thickness increases, the FWHM for each resonance decreases.

Figure 10 shows the frequency shift and the change in the absorption index relative to the initial resonance position. These values were calculated by the formulae

$$F_{\text{shift}} = F_{\text{without film}} - F_{\text{with film}}, \quad (7)$$

$$A_{\text{shift}} = A_{\text{with film}} - A_{\text{without film}}, \quad (8)$$

where $F_{\text{without film}}$ and $A_{\text{without film}}$ are the frequency and absorption index at the resonance frequency in the absence of a film, respectively; and $F_{\text{with film}}$ and $A_{\text{with film}}$ are the frequency and absorption index at the resonance frequency in the presence of a film.

Note that at a frequency of 0.85 THz, the absorption index of the histidine film is lower than the absorption index in the absence of the film. This nonlinearity can be associated with the presence of a characteristic histidine resonance at a frequency of 0.79 THz. The resonance at a frequency of 0.85 THz is more sensitive to changes in the thickness of the RBD S protein film.

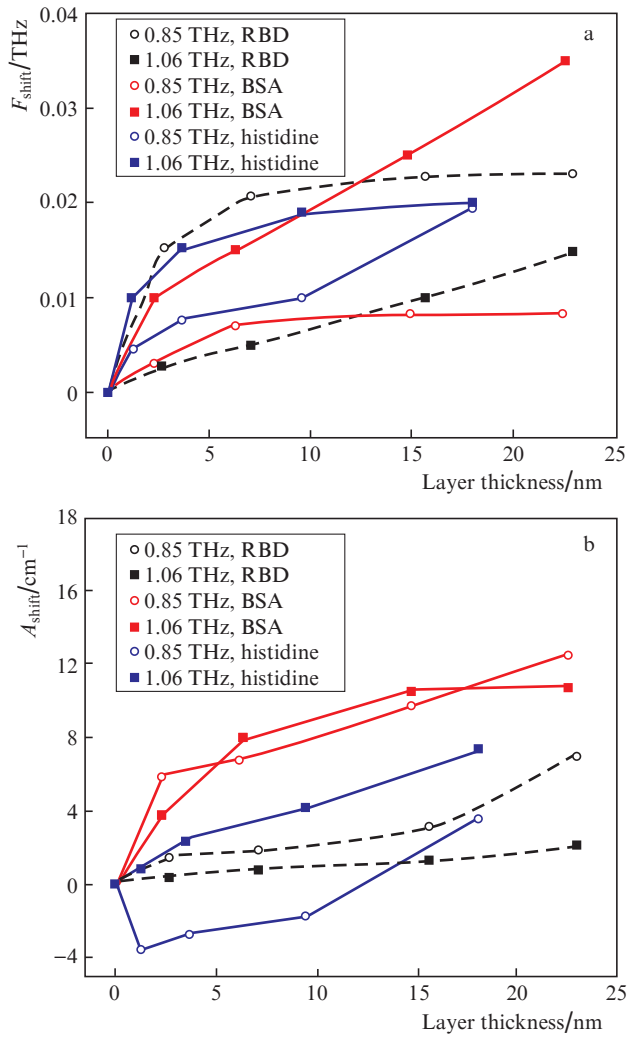

Figure 10. (Colour online) (a) Frequency shift of resonances F_{shift} and (b) change in the absorption index of A_{shift} relative to the initial position of the metastructure resonances depending on the thickness of the histidine, BSA, and RBD films. The results were obtained by averaging over three independent measurements with an error of 5%–6% for each experimental point.

3.4. Determination of the adhesion efficiency of organic films by THz-TDS and spectrophotometry

The proposed method for determining the adhesion efficiency of the RBD S protein on the metastructure surface is based on a comparison of two independent measurement results obtained by THz -TDSy and spectrophotometry in the region of 185–1800 nm. The metastructure transmission after each stage of film extraction was measured by THz-TDS, while the transmission of a 1-cm liquid layer in which the films were extracted was measured with a spectrophotometer (UV-3600, Shimadzu, Germany). Film extraction is understood as the

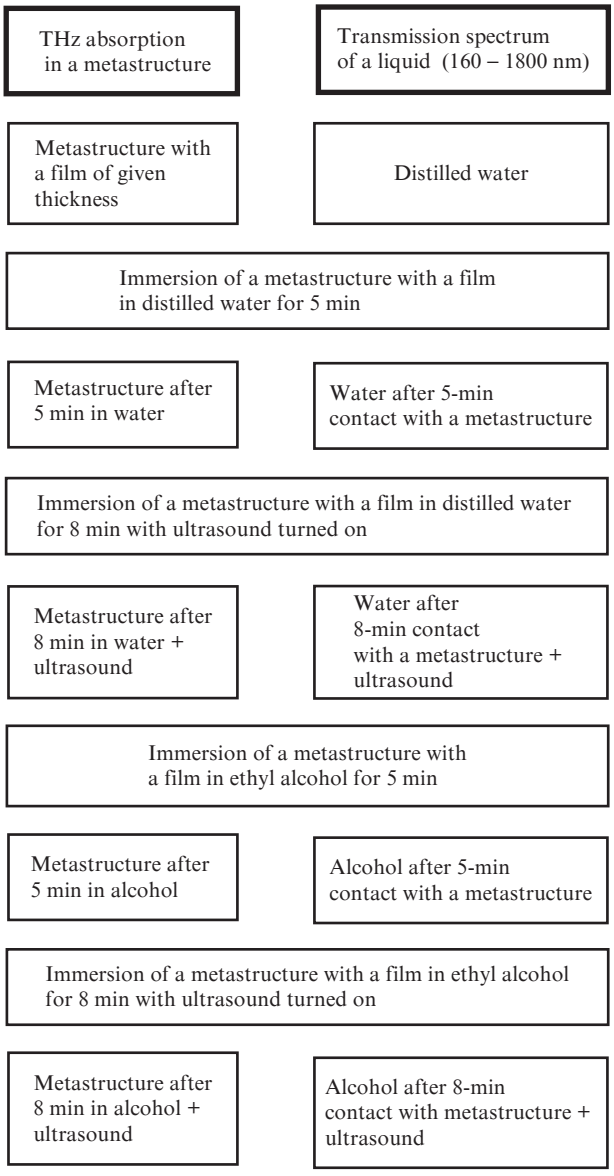

Figure 11. Protocol of sequential extraction and measurement of THz absorption of the metastructure, as well as measurement of the liquid transmission by the spectrophotometric method.

process of immersing a metastructure with a film into a liquid for a specified time. The extraction times in liquids were obtained experimentally. The stages of extraction and THz absorption measurements of the metastructure with deposited films, as well as the process of spectrophotometric transmission measurements of solution after extraction, is summarised in the protocol shown in Fig. 11.

The THz absorption spectra of the metastructure upon successive film extraction are shown in Fig. 12. Resonances of absorption indices approach the resonances characteristic of a pure metastructure at each extraction stage. Changes in the absorption index and the position of resonances of the metastructure during sequential extraction were calculated using Eqns (7), (8) and are shown in Fig. 13. The thicknesses of the films after the extraction stages were not measured. It can be seen from Fig. 13 that a shift of absorption resonances is observed at each stage of extraction. Note that the frequency shifts for resonance at a frequency of 0.85 THz and changes in the absorption index for resonance at a frequency of 1.06 THz are more sensitive to the RBD extraction process.

The transmission spectra of liquids after each stage of extraction, obtained using the spectrophotometric method in the range 185–1800 nm, are shown in Fig. 14. To determine the concentration C_{ex} of substances extracted from the surface of the metastructure, we measured the transmission of histidine solutions with concentrations of 0.06–0.01 mg mL^{-1} at $\lambda = 211$ nm, as well as BSA and RBD with concentrations of 1.0–0.02 mg mL^{-1} and 2.2–0.01 mg mL^{-1} , respectively, at $\lambda = 280$ nm. The obtained dependence of the concentration of the solution on the transmission made it possible to calculate the concentrations of proteins extracted from the metastructure (RBD S protein and BSA) and histidine in solutions according to the formula

$$C_{ex} = \frac{D}{k}, \tag{9}$$

where the concentration of C_{ex} is taken in mg mL^{-1}; $D = \lg(I_0/I)$ is the optical density at $\lambda = 210$ nm for histidine and at $\lambda = 280$ nm for BSA and RBD; I_0 and I are the intensities

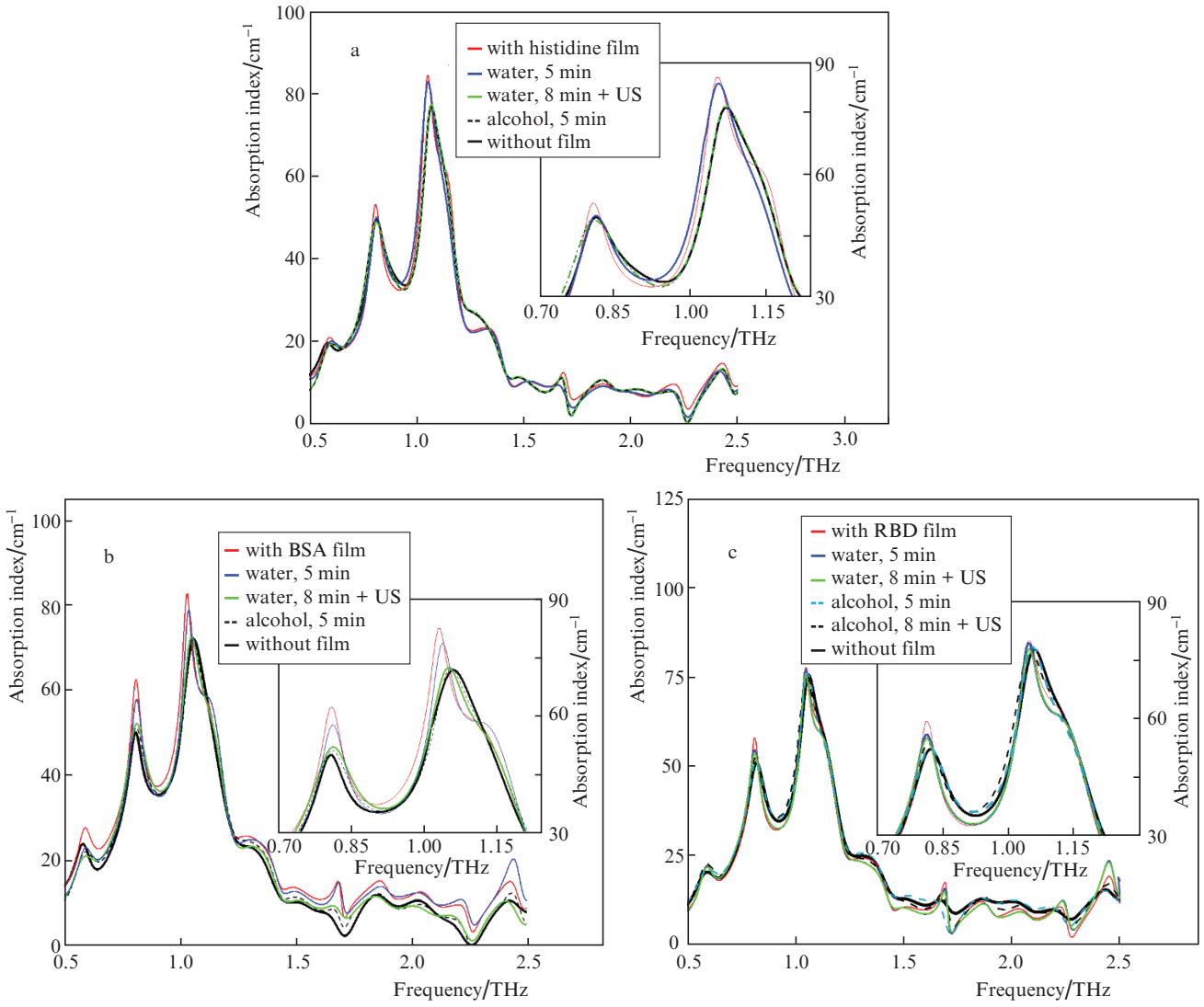

Figure 12. (Colour online) Absorption index of the metastructure with (a) histidine, (b) BSA, and (c) RBD films in the THz range with sequential extraction in water and alcohol.

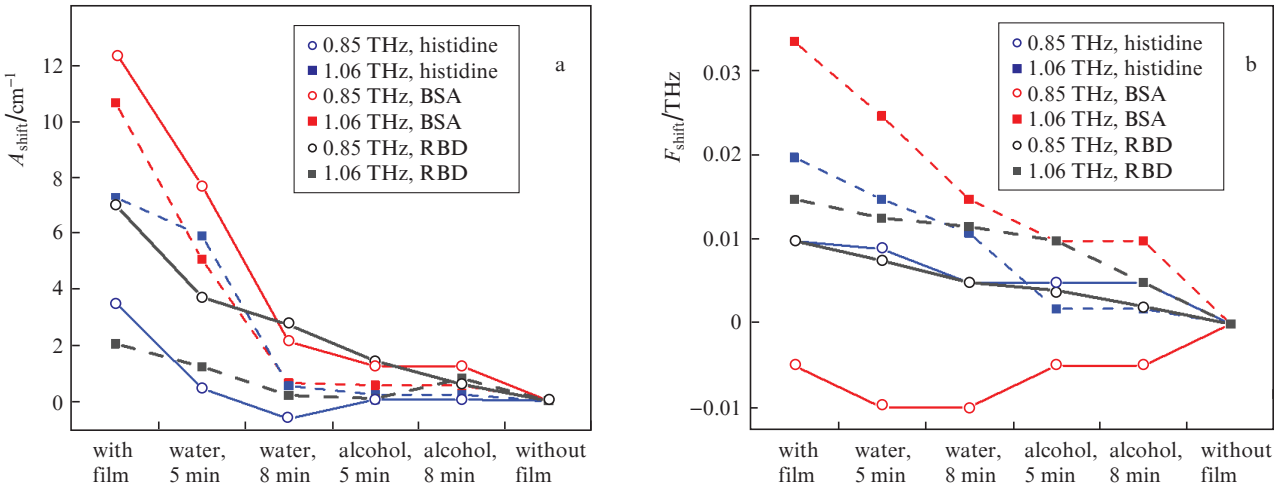

Figure 13. (Colour online) (a) Change in the THz absorption index A_{shift} and (b) frequency shift of THz resonances F_{shift} of the metastructure during sequential extraction of sample layers from the surface of the metastructure. The horizontal axis indicates the stages of extraction. The results were obtained by averaging over three independent measurements with an error of 5%–6% for each experimental point.

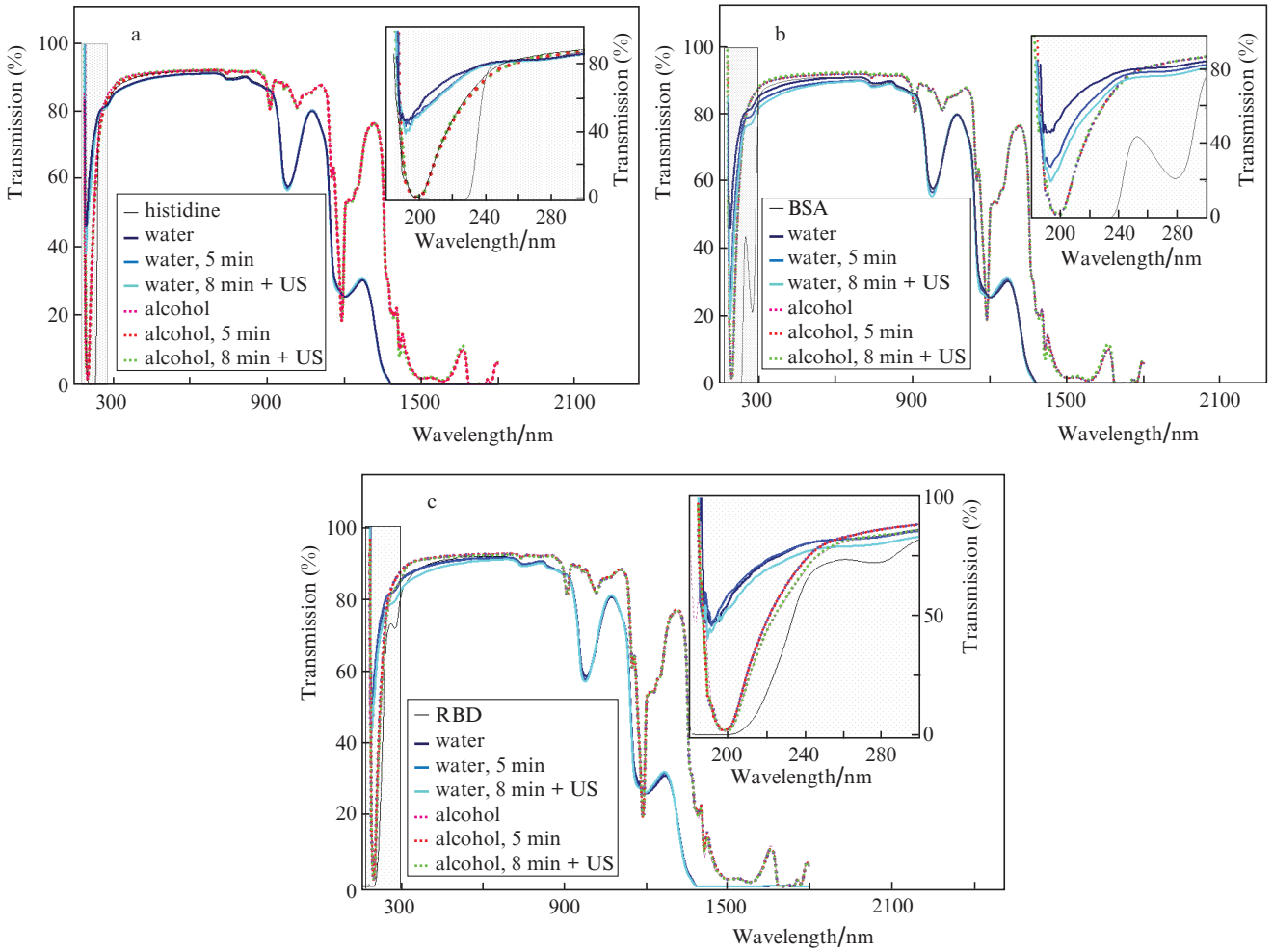

Figure 14. (Colour online) Transmission spectra of liquids in contact with the metastructure with (a) histidine, (b) BSA, and (c) RBD films.

of the incident and transmitted radiation, respectively; and k is the slope of transmission versus solution concentration curve, which was 0.0316 for RBD (λ = 280 nm), 40.7 for histidine (λ = 210 nm), and 0.597 for BSA (λ = 280 nm).

To compare the concentrations of proteins extracted from the metastructure (RBD S protein and BSA) and histidine in solutions, they were normalised to the initial concentration of the solution using the formula $C = (C_{ex}/C_{init}) \times 100\%$, where

C_{init} are the concentrations of initial solutions in mg mL^{-1}. The concentrations of proteins washed off from the metastructure (RBD S protein and BSA) and histidine in solutions after each extraction stage are shown in Fig. 15. It can be seen that BSA and histidine are more strongly extracted into the liquid at the first extraction stage (5 min in water), and changes in concentrations at the last extraction stage [8 min in alcohol with cleaning by ultrasound (US)] are insignificant compared to the previous stage. This can be interpreted as the cleaning of the metastructure from BSA and histidine films below their detection threshold. For RBD, an inverse relationship is observed: significant changes in concentration occur at the stages of ultrasonic cleaning both in water and in alcohol. Note that insignificant changes in concentration relative to the previous stage of extraction for RBD are observed later, which indicates a higher efficiency of adhesion of this substance to the metastructure as compared to BSA and histidine.

Also, from Fig. 15, the total concentration of proteins extracted from the metastructure (RBD S protein and BSA) and histidine in water and alcohol solutions was qualitatively determined, which was 2.4% for histidine, 6.1% for BSA, and 28.2% for RBD. Analysis of the obtained total concentrations shows that the conclusion about a relatively high efficiency of RBD adhesion is not obvious in the absence of joint THz absorption measurements of metastructures with deposited film substances, since a low total concentration (for histidine and BSA) may indicate that the substance is not extracted by the selected methods. However, the position of the THz resonance and the absorption index are restored faster for metastructures with deposited BSA and histidine films, which confirms the qualitative results of spectrophotometry and the conclusion about the relatively high efficiency of RBD adhesion.

Analysis of the change in the absorption index and the frequency shift of THz resonances of metastructures during sequential film extraction shows that the resonances of the metastructure are restored faster for histidine and BSA, than for RBD. It is important to note that the restoration of the resonance frequency and absorption index for metastructure resonances occurs by 95%, which imposes restrictions on the permissible number of operations of the metastructure. We assume that the incomplete restoration of the spectra may be associated with the presence of residual molecules on the metastructure; however, repeated immersion of pure structures in the liquid does not cause any changes in both the spectrophotometric results and the results of THz absorption measurements of the metastructure.

An independent experiment using the spectrophotometric method confirms the results obtained by the THz-TDS. Changes in the concentration of RBD solutions are observed after all extraction stages, while for histidine and BSA, there are no changes in concentration after the extraction stage, which includes immersion in water with ultrasonic cleaning.

4. Conclusion

In this work, we investigated the features of the RBD S protein of the SARS-CoV-2 virus adsorption on surfaces by vibrational spectroscopy using THz metamaterials. The IR spectra of the RBD S protein obtained from the CHO culture were measured for the first time. A comparative study of the THz spectra of the RBD S protein, BSA protein, and amino acid histidine was carried out. To increase the sensitivity of THz-TDS, we have developed a THz metastructure that is spectrally sensitive to the presence of the RBD S protein, BSA protein, and the amino acid histidine on its surface. Terahertz spectroscopy was used to study thin films of histidine, BSA, and RBD on the surface of the metastructure. The metastructure absorption spectra in the presence of each type of films under study demonstrate clearly distinguishable topological differences, which show resonance frequency shifts and absorption index changes with increasing film thickness. An original technique for studying the adhesion properties of

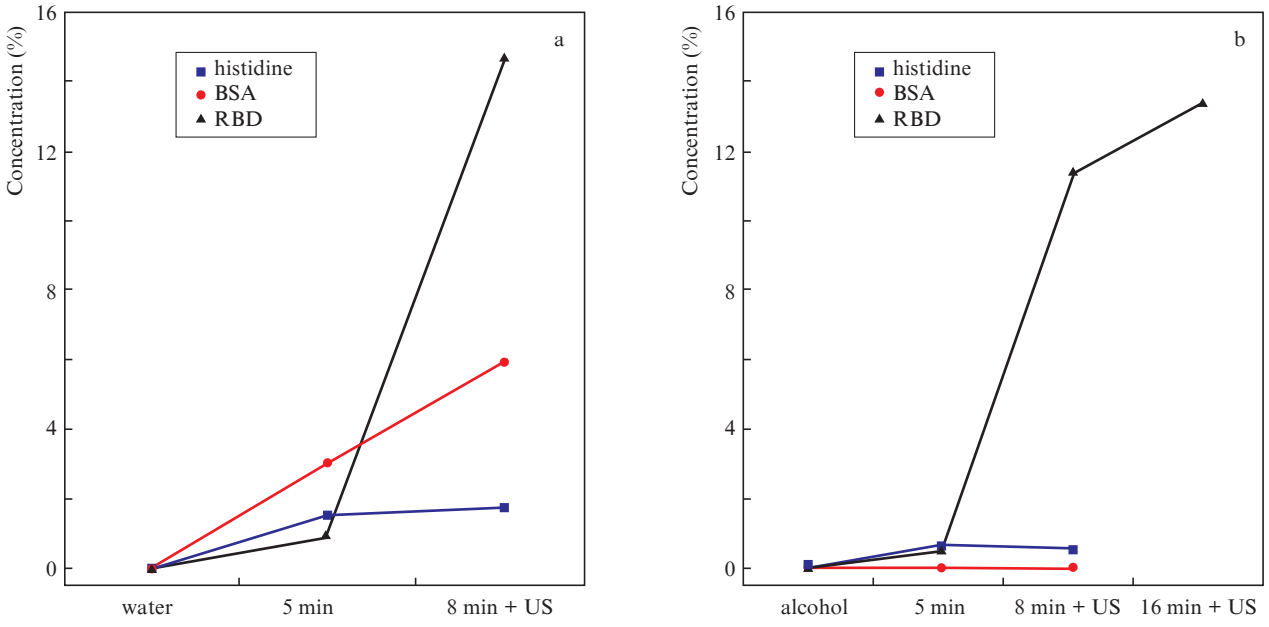

Figure 15. (Colour online) Concentration of proteins washed off from the metastructure (RBD S protein and BSA) and histidine in solutions at each stage of extraction: extraction (a) in water and (b) in ethyl alcohol. The horizontal axis shows the stages of extraction.

RBD is proposed, based on an independent comparison of the spectral characteristics of the metastructure during sequential extraction of the deposited film. When comparing the adhesion properties of histidine, BSA, and RBD by THz spectroscopy using a metastructure, it was revealed that RBD has the most effective adhesion among the set of three studied substances. The high adhesion efficiency of RBD is also qualitatively confirmed by an independent spectrophotometric method.

Acknowledgements. This work was supported by the Russian Foundation for Basic Research (Grant No. 20-04-60505), the Ministry of Science and Higher Education of the Russian Federation within the framework of the State Assignment for the Branch of the Federal Research Centre 'Crystallography and Photonics' of RAS (Grant No. 075-15-2019-1950), the Interdisciplinary Scientific and Educational School of Moscow University "Photonic and Quantum Technologies. Digital Medicine", as well as by a grant under the Decree of the Government of the Russian Federation No. 220 dated April 9, 2010 (Agreement No. 075-15-2021-615 dated 4 June 2021).

References

1. Javier A.J. et al. *J. Mol. Biol*., **432** (10), 3309 (2020); DOI:10.1016/j.jmb.2020.04.009.
2. Generalov I.I., Zheleznyak N.V., Okulich V.K., Frolova A.V., Zubareva I.V., Moiseeva A.M., Senkovich S.A., Shilin V.E., Denisenko A.G., Generalova A.G. *Meditsinskaya virusologiya: uchebnoe posobie* (Medical Virology: Textbook) (Vitebsk, VSMU, 2017).
3. Sungnak W., Huang N., Bécavin C., et al. *Nat. Med*., **26**, 681 (2020); https://doi.org/10.1038/s41591-020-0868-6.
4. Sohail A., Nutini A. *Prog. Biophys. Mol. Biol*., **155**, 29 (2020). DOI:10.1016/j.pbiomolbio.2020.04.002.
5. Walls A.C. et al. *Cell*, **181** (2), 281 (2020). DOI:10.1016/j.cell.2020.02.058.
6. Joonaki E. et al. *Chem*, **6** (9), 2135 (2020). DOI:10.1016/j.chempr.2020.08.001.
7. Smolyanskaya O.A., Chernomyrdin N.V., Konovko A.A., et al. *Prog. Quantum Electron*., **62**, 1 (2018); https://doi.org/10.1016/j.pquantelec.2018.10.001.
8. Doremalen N. et al. *New Engl. J. Med*., **382** (16), 1564 (2020). DOI:10.1056/NEJMc2004973.
9. Barth A. *Biochim. Biophys. Acta Bioenerg*., **1767** (9), 1073 (2007). DOI:10.1016/j.bbabio.2007.06.004.
10. Mankova A.A., Cherkasova O.P., Lazareva E.N., et al. *Opt. Spectrosc*., **128** (7), 964 (2020); https://doi.org/10.1134/S0030400X20070115 [*Opt. Spektrosk*., **128** (7), 956 (2020); https://doi/10.21883/OS.2020.07.49568.73-20].
11. Byrne H.J., Bonnier F., et al. *Clin. Spectrosc*., **2**, 100004 (2020).
12. Kochan K. et al. *Appl. Spectrosc*., **75** (6), 611 (2021). DOI:10.1177/ 0003702820985856.
13. Wei L. et al. *Front. Lab. Med*., **2**, 127 (2018).
14. Elyashevich M.A. *Atomnaya i molekulyarnaya spektroskopiya* (Atomic and Molecular Spectroscopy) (Moscow: KomKniga, 2006).
15. Lin S. et al. *IEEE J. Sel. Top. Quantum Electron*., **27** (4), 6900207 (2021). DOI:10.1109/JSTQE.2020.3038308.
16. Gu H., Shi C., Wu X., et al. *Analyst*, **145** (20), 6705 (2020).
17. Peng Y., Shi C., Zh Y., et al. *PhotoniX*, **1**, 12 (2020); https://doi.org/10.1186/s43074-020-00011-z.
18. Maier S.A. *Plasmonics: Fundamentals and Applications* (New York: Springer, 2007).
19. Pilot R., Signorini R., Durante C., Orian L., Bhamidipati M., Fabris L. *Biosensors*, **9** (2), 57 (2019). DOI:10.3390/bios9020057.
20. Neubrech F., Huck C., Weber K., Pucci A., Giessen H. *Chem. Rev*., **117** (7), 5110 (2017). DOI:10.1021/acs.chemrev.6b00743.
21. Huang Y., Ho H., Kon S., Kabashin A. *Ann. Phys*., **524**, 637 (2012).
22. Zhou H., Yang C., Hu D., Li D., Hui X., Zhang F., Mu X. *Appl. Phys. Lett*., **115** (14), 143507 (2019). DOI:10.1063/1.5111584.
23. Cherkasova O., Peng Y., Konnikova M., Kistenev Y., Shi C., Vrazhnov D., Shkurinov A. *Photonics*, **8** (1), 22 (2021). DOI:10.3390/photonics8010022.
24. Park S., Hong J., Choi S., et al. *Sci. Rep*., **4**, 4988 (2014); https://doi.org/10.1038/srep04988.
25. Pendry J.B., Holden A.J., Robbins D.J., Stewart W.J. *J. Phys. Condens. Matter*, **10** (22), 4785 (1998).
26. Konnikova M., Cherkasova O.P., Nazarov M.M., Vrazhnov D.A., Kistenev Yu.V., Titov S.E., Kopeikina E.V., Shevchenko S.P., Shkurinov A.P. *Biomed. Opt. Express*, **12**, 1020 (2021).
27. Nazarov M.M., Cherkasova O.P., Shkurinov A.P. *J. Infrared Millim. Terahertz Waves*, **39**, 840 (2018); https://doi.org/10.1007/s10762-018-0513-3.
28. Acree W., Chickos J.S. *J. Phys. Chem. Ref. Data*, **39** (4), 043101 (2010). DOI:10.1063/1.3309507.
29. Kreb J. *Spectroscopic Ellipsometry on Thin Films of TiO_2: Comparing Cauchy and Cody-Loretnz Models in CompleteEASE* (Oregon State University, 2020).
30. Naftaly M., Miles R.E. *J. Appl. Phys*., **102**, 043517 (2007); https://doi.org/10.1063/1.2771049.
31. Pandey Sh., Gupta B., Chanana A., Nahata A. *Adv. Phys. X*, **1** (2), 176 (2016). DOI: 10.1080/23746149.2016.1165079.
32. Pendry J.B., Holden A.J., Robbins D.J., Stewart W.J. *IEEE Trans. Microwave Theory Tech*., **47** (11), 2075 (1999). DOI:10.1109/22.798002.
33. Singh R., Smirnova E., Taylor A.J., O'Hara J.F., Zhang W. *Opt. Express*, **16**, 6537 (2008).
34. He Y., Qi J., Xiao L., Shen L., Yu W., Hu T. *Eng. Life Sci*., **21**, 453 (2021); https:// doi.org/10.1002/elsc.202000106.
35. Nazarov M.M., Cherkasova O.P., Shkurinov A.P. *Quantum Electron*., **46** (6), 488 (2016) [*Kvantovaya Elektron*., **46** (6), 488 (2016)].
36. Nazarov M., Cherkasova O., Shkurinov A. *EPJ Web Conf*., **195**, 10008 (2018).
37. Cherkasova O., Nazarov M., Shkurinov A. *J. Phys. Conf. Ser*., **793**, 012005 (2017).
38. Withayachumnankul W., Abbott D. *IEEE Photonics J*., **1** (2), 99 (2009). DOI: 10.1109/JPHOT.2009.2026288.
39. Yu Y., Lin Y.-S. *Results Phys*., **13**, 102321 (2019). DOI:10.1016/j.rinp.2019.102321.